Materials Advances

ROYAL SOCIETY OF CHEMISTRY

PAPER

View Article Online
View Journal | View Issue

Cite this: *Mater. Adv.*, 2022, 3, 7894

$Cs_2Ag_xNa_{1-x}Bi_yIn_{1-y}Cl_6$ perovskites approaching photoluminescence quantum yields of 100%†

Oleksandr Stroyuk,*[a] Oleksandra Raievska,[a] Anastasia Barabash,[b] Christian Kupfer,[b] Andres Osvet,[b] Volodymyr Dzhagan,[cd] Dietrich R. T. Zahn,[ef] Jens Hauch[ab] and Christoph J. Brabec[ab]

Received 24th June 2022,
Accepted 21st August 2022

DOI: 10.1039/d2ma00737a

rsc.li/materials-advances

A new single-step and green approach for the synthesis of microcrystalline $Cs_2Ag_xNa_{1-x}Bi_yIn_{1-y}Cl_6$ (CANBIC) perovskites in ambient conditions is introduced. The CANBIC powders emit broadband self-trapped excitonic photoluminescence (PL) with a champion PL quantum yield (QY) of 98 ± 2% and a PL lifetime of *ca.* 2 μs observed for x = 0.40 and y = 0.01–0.02. The study focuses on the dependence of structural, spectral, and photophysical properties of CANBICs on Bi content. CANBICs are solid solutions with isomorphous In-to-Bi substitution with the bandgap and valence band edge energy decreasing gradually with increasing y. The PL QY and the rate constant of the radiative recombination showed volcano-shaped dependences on the Bi content, while the rate of the non-radiative recombination revealed a drastic growth by three orders of magnitude as the Bi fraction y was elevated from 0.01 to 1.0 indicating that $BiCl_6$ units are responsible for non-radiative recombination.

Introduction

The tremendous progress in the field of light conversion using lead-halide perovskite compounds achieved within an unprecedentedly short time period[1–4] stimulated a massive advancement in many related areas, including exploration of tandem perovskite-based photovoltaic materials,[1,2,4–6] search for low-dimensional (2D, 0D) forms of halide perovskite absorbers,[1,4,5,7–12] as well as attempts to develop lead-free perovskite compounds with light harvesting properties comparable with those of lead-halide perovskites.[1,3,4,8,12–16] The latter research direction highlighted many promising compounds, either directly stemming from lead-based ancestors, such as tin-halide perovskites,[3,8,12–16] or those belonging to a family of double-cation perovskites $A_2^IM^IM^{III}X_6$, where A is an alkali cation, X is a halide, and the couple of M^I and M^{III} represents an isovalent substitution of two Pb^{II} cations in the lead-halide $(APbX_3)_2$ perovskite structure.[3,8,12–16]

The double lead-free compounds combine the variability of A and X sites typical for $APbX_3$ compounds with new possibilities of independent variation of both M^I and M^{III} sites, which has no analogs in the chemistry of lead-halide perovskites and imparts the double perovskites with a unique compositional flexibility.[3,8,12–16] In particular, candidates for M^I and M^{III} sites can be selected from $M^I = Na^+, K^+, Ag^+, Tl^+, Au^+$, *etc.* and $M^{III} = In^{3+}, Bi^{3+}, Sb^{3+}, Fe^{3+}, Au^{3+}$, *etc.*, varied independently, and together with A^I and X components yield many thousands of possible compositions.[3,8,12–16]

Among the double halide perovskites, compounds based on Bi^{III} and In^{III} with a general formula $Cs_2Ag_xNa_{1-x}Bi_yIn_{1-y}Cl_6$ (abbreviated as CANBIC by the first letters of the elements) occupy an outstanding position due to a combination of the compositional variability, stability, and promising light-conversion properties, in particular, highly efficient broadband photoluminescence (PL).[12,13,15,17–42] These compounds typically feature a dome-shaped dependence of many photophysical characteristics (PL efficiency and lifetime, electron–phonon coupling strength, *etc.*) on the ratios of Ag/Na and Bi/In.[17,18,20,21,23,34] For example, CANBIC compounds often show exceptionally

[a] *Forschungszentrum Jülich GmbH, Helmholtz-Institut Erlangen Nürnberg für Erneuerbare Energien (HI ERN), 91058 Erlangen, Germany. E-mail: o.stroyuk@fz-juelich.de*
[b] *Friedrich-Alexander-Universität Erlangen-Nürnberg, Materials for Electronics and Energy Technology (i-MEET), Martensstrasse 7, 91058 Erlangen, Germany*
[c] *V. Lashkaryov Institute of Semiconductors Physics, National Academy of Sciences of Ukraine, 03038 Kyiv, Ukraine*
[d] *Physics Department, Taras Shevchenko National University of Kyiv, 60 Volodymyrs'ka str., 01601 Kyiv, Ukraine*
[e] *Semiconductor Physics, Chemnitz University of Technology, 09107 Chemnitz, Germany*
[f] *Center for Materials, Architectures and Integration of Nanomembranes (MAIN), Chemnitz University of Technology, 09107, Chemnitz, Germany*

† Electronic supplementary information (ESI) available: Detailed descriptions of the procedures of CANBIC synthesis, purification, and preparation of samples for structural and spectral studies; details of the characterization methods; description of the calculation of recombination rate constants; collections of SEM images and XRD patterns of CANBICs with different Bi content; results of PL QY measurements in different conditions; collection of XPS data for Ag, In, and Bi elements in CANBICs; positions of VB/CB levels; vibrational parameters of CANBIC; composition of CANBICs determined by XPS. See DOI: https://doi.org/10.1039/d2ma00737a

strong dependence of the PL quantum yield (QY) and Huang–Rhys factor on the Ag-to-Na ratio x,[18,21,25,28–30,32,34] while CANBICs with a fixed x typically reveal a dome-shaped dependence of the PL efficiency on the Bi fraction y.[17,18,31,32,34,41]

Along with the variable parameters x and y, both Cs and Cl sites can also be varied and potentially substituted by analogs (for example, Cs by Rb or methylammonium). This fact strongly multiplies the number of possible compositions opening a vast field for the search of new effects and unexpected compositional dependences of functional properties relevant for applications in light conversion and emission (bandgap, PL QY, charge carrier density, mobility, lifetime, *etc.*).

At the same time, the potential and capacities of such a search are considerably limited by the current level of development of synthetic approaches to CANBIC perovskites. Typical synthetic protocols are rather unflexible and energy-consuming, requiring the presence of concentrated HCl[8,16,18,19,21,28,31,32,41,42] or application of prolonged hydrothermal treatments and/or annealings.[8,16,18,19,26] Attempts to make the synthesis of CANBICs and related compounds more environmentally friendly by mimicking syntheses of lead-based halide perovskites, such as antisolvent- or oversaturation-induced crystallization, either yield mixtures of multiple phases with a low control over the crystallization dynamics[16,32,33,43] or do not cover the entire possible ranges of compositions.[32,43] In this view, further search for mild and fast and, at the same time, highly controllable protocols for the synthesis of CANBIC perovskites remains a topic of high relevance.

CANBIC compounds are regarded as a green and sustainable Pb-free representative for the class of halide perovskites. However, green and sustainable should not only refer to the material, but also to the synthesis. Recently, we reported a communication on a relatively green single-step synthesis of luminescent CANBIC perovskites in 2-propanol:water mixtures at ambient conditions without any additional thermal treatments necessary to achieve high PL efficiencies and stability.[44] Here, a more detailed and comprehensive report on the structural, spectral, and photophysical characteristics of CANBIC perovskites produced by this approach is provided focusing on the dependence of CANBIC properties on the Bi-to-In ratio, while other possible variables are kept constant. A fine tuning of the synthesis conditions is shown to enhance the PL QY of the most emissive CANBIC samples almost to unity.

Results and discussion

A green synthesis of CANBIC perovskites implies minimizing both the energy input and utilization of aggressive/volatile compounds (concentrated HCl, organic solvents), but still maintaining a reliable control over the composition of the products. In line with these criteria, a protocol for the synthesis of microcrystalline CANBIC compounds was developed allowing the perovskites of any given composition to be precipitated under ambient conditions with no necessity of thermal post-treatment to improve crystallization (hydrothermal treatment, annealing, *etc.*). The synthesis is a single-step procedure and requires interaction of two precursors containing metal ions in 2-propanol:water mixtures and a minimal amount of HCl necessary to prevent hydrolytic by-reactions of In^{III} and Bi^{III}.

To steer the reaction to the formation of a single perovskite phase with no noticeable admixtures of other possible by-products the metal cations were separated between two precursors and their reactivity equalized. In particular, Bi^{3+} and In^{3+} were bound into complexes with HCl in precursor 1, while Cs^+, Na^+, and Ag^+ were separated into precursor 2 where ammonia was added to avoid hydrolysis of Ag^+ in a mildly alkaline medium produced by the presence of cesium and sodium acetates. The feasibility and some details on the synthesis were discussed in our recent communication,[44] where the maximal PL efficiency of CANBIC perovskites was achieved at 2% content of Bi^{III} and a molar fraction of silver of 0.35.

Here a broader characterization of the structure, spectral, and photophysical properties of CANBIC perovskites produced by such an approach is provided with a focus on the variation of the content of bismuth. The molar Bi fraction y was varied from 0.05% to 100% while tracking the influence of the bismuth-to-indium ratio y on the morphology, structure, spectral, and photophysical properties of CANBIC perovskites.

With the bismuth content varied, all other parameters are maintained identical, in particular by retaining a constant nominal silver-to-sodium ratio $x = 0.40$, as well as by providing excesses of Cs^+ and Na^+ during the synthesis and by performing the synthesis at room temperature (22 °C). In the following discussion the CANBICs with a varied Bi content are referred to either by the value of y (implying that $x = 0.40$) or by abbreviating the perovskites as CANBIC-Y%, where $Y = 0.05$–100. All the properties of CANBIC perovskites are primarily discussed in the present paper as functions of the molar Bi^{III} fraction y.

The details of the synthesis and purification of CANBIC perovskites as well as methods of structural and optical characterization are provided in ESI.†

In the following discussion we provide an account on the structural, spectral, and photophysical properties of CANBIC perovskites with a varied Bi-to-In ratio investigated with appropriate techniques. First, morphology, composition and structure of CANBICs are probed by a combination of scanning electron microscopy (SEM), energy-dispersive X-ray spectroscopy (EDX), and X-ray diffraction (XRD). Basing on these results we then discuss spectral characteristics of CANBICs, including light absorption and emission, PL efficiency and factors affecting PL QY, positions of valence band (VB) and conduction band (CB) as functions of the Bi content revealed by X-ray photoelectron spectroscopy (XPS), as well as vibrational properties of CANBICs probed by non-resonant Raman spectroscopy. Finally, the kinetics of the photophysical processes in CANBIC perovskites is addressed by analyzing time-resolved PL decay traces of the samples with a variable Bi-to-In ratio.

1 Composition, morphology, and structure of CANBIC perovskites

1.1 Probing morphology and composition of CANBICs by SEM/EDX. The precipitation of CANBICs in 2-propanol:water

mixtures in the presence of diluted HCl results in microcrystalline products showing a large dispersion of crystal sizes and mostly polygonal crystal shape (Fig. 1, columns 1,2). The Bi fraction was found to exert a moderate effect on the CANBIC crystal size. $Cs_2Ag_{0.4}Na_{0.6}InCl_6$ (CANIC) perovskite containing no Bi^{III} shows the largest grain size of all tested samples, *ca.* 2–5 μm (Fig. S1, ESI† $y = 0$). When the minimal amount of Bi^{III} is introduced into the perovskite structure ($y = 0.005$), a fraction of smaller (*ca.* 0.5 μm) crystals can be observed in SEM images accompanying the major fraction of larger crystals (Fig. S1, ESI† $y = 0.005$). As the Bi content is further increased, the crystal size decreases noticeably and steadily from *ca.* 2–3 μm for $y = 0.02$ to *ca.* 0.5–1.0 μm for $y = 0.7$ and below this range for the lowest In content at $y = 0.9$ (Fig. S1, ESI† $y = 0.02$–0.9). For the pure $Cs_2Ag_{0.4}Na_{0.6}BiCl_6$ (CANBC) perovskite with $y = 1.0$ the crystal size grows again to *ca.* 1–3 μm.

During SEM inspection CANBIC samples were found to emit intense cathodoluminescence (CL) under irradiation with the electron beam. The highest CL intensity was observed at $y = 0.02$ gradually decreasing again for higher bismuth contents.

The high intensity of CL allows the CANBIC crystals to be clearly observed in SEM using only the CL contrast already at 10 kV accelerating voltage (compare columns 2 and 3 in Fig. 1). At that, the shape of the crystals is identical for SEM and CL images with no dark areas observed in CL images indicating a high structural homogeneity of the tested samples.

Selected probing of the samples in different random points by EDX revealed constant compositions close to the nominal ones set at the synthesis (Fig. 1, column 4) with no noticeable variations among the tested points.

Statistically significant information on the elemental composition of CANBIC samples was collected by probing the samples with y varied from 0 to 1.0 by EDX in 7–10 different areas for each composition (Table 1). The real composition of the CANBIC samples after all treatments and purification was found to be very close to the nominal one (set at the synthesis) showing a good control over the CANBIC composition by tuning the composition of both starting precursors. In particular, the Bi content closely followed the nominal y value, the silver fraction x was found to be quite close to 0.40 varying by about ±5%.

Table 1 Elemental composition of CANBIC perovskites with $x = 0.4$ and varied Bi content

Nominal y	N_{EDX}	Real y	Real x	Cs-to-M ratio	Cl-to-M ratio
0	8	0	0.35 ± 0.10	2.1 ± 0.1	5.8 ± 0.3
0.005	8	0.02 ± 0.02	0.37 ± 0.07	2.2 ± 0.2	6.0 ± 0.3
0.02	7	0.02 ± 0.01	0.35 ± 0.10	2.1 ± 0.1	6.2 ± 0.3
0.10	8	0.11 ± 0.02	0.42 ± 0.08	2.2 ± 0.1	5.9 ± 0.1
0.20	9	0.23 ± 0.04	0.43 ± 0.05	2.1 ± 0.1	5.8 ± 0.2
0.30	8	0.32 ± 0.03	0.45 ± 0.05	2.2 ± 0.2	5.7 ± 0.2
0.50	8	0.51 ± 0.05	0.43 ± 0.08	2.1 ± 0.2	5.5 ± 0.2
0.70	10	0.70 ± 0.04	0.46 ± 0.06	2.0 ± 0.1	5.4 ± 0.1
0.90	8	0.90 ± 0.03	0.40 ± 0.07	2.1 ± 0.3	5.8 ± 0.2
1.00	8	0.99 ± 0.01	0.47 ± 0.06	2.1 ± 0.2	5.3 ± 0.4

Notes: N_{EDX}, number of EDX spectra processed for the statistical analysis.

The ratio of Cs to the sum of M = Bi + In was near the expected value of 2 despite the presence of an excess of Cs^+ at the synthesis. The ratio of chlorine to the sum of M = Bi + In was close to 6 as expected for the CANBIC stoichiometry (Table 1).

The composition of CANBIC crystals with varied Bi content ($y = 0.1$) was complementary identified by X-ray photoelectron spectroscopy (see an exemplary survey spectrum and summary of the results in Fig. S2 and Table S1, ESI† respectively), showing a good correspondence with the EDX measurements.

1.2 Probing structure of CANBIC perovskites by XRD. The XRD patterns of CANBIC perovskites show the characteristic cubic pattern of perovskites with a *Fm*3*m* lattice symmetry[17–21,26,28,32] general for all tested samples irrespective of the Bi content (Fig. 2a) with no additional peaks. These observations indicate a high phase purity of the samples.

The XRD patterns were subjected to a Rietveld refinement to trace the dependence of the lattice parameter L on the Bi fraction y. This dependence was found to be linear (Fig. 2b) with the lattice parameter increasing from 10.515(2) Å for

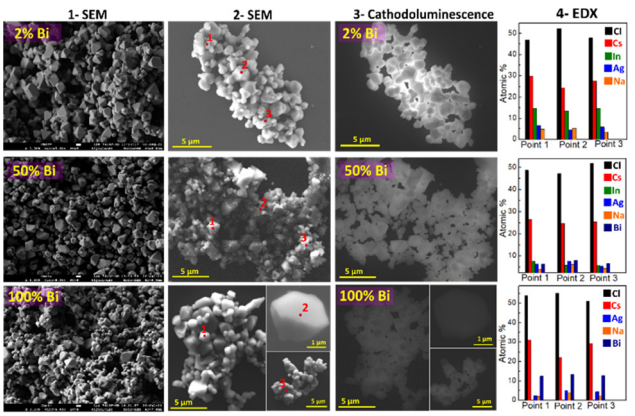

Fig. 1 SEM microphotographs of CANBIC microcrystals made by using the secondary electrons contrast (columns 1 and 2) and the cathodoluminescence contrast (column 3) as well as elemental composition in selected points determined by EDX (column 4).

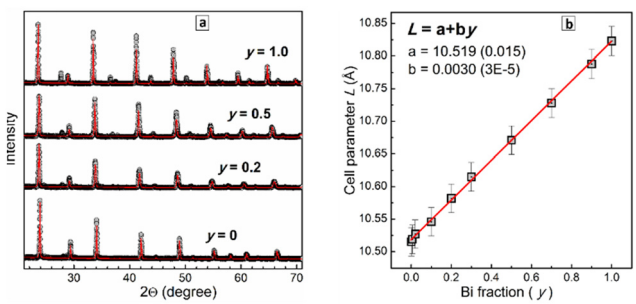

Fig. 2 (a) X-Ray diffractograms of CANBIC perovskites with $x = 0.4$ and $y = 0$, 0.2, 0.5, and 1.0. Gray circles correspond to experimental data, red solid lines are the results of Rietveld refinement. (b) Cell parameter of CANBIC perovskites as a function of Bi fraction y. Gray squares are experimental data, red line represents a linear fit (fitting parameters a and b are presented in figure).

CANIC (y = 0) to 10.823(2) Å for CANBC (y = 1.0) reflecting the gradual lattice expansion due to the larger ionic radius of Bi^{3+} as compared to In^{3+}.[17,18,20,26,28,32] The linear character of $L(y)$ obeying Vegard's law shows that the CANBIC perovskites are ideal solid solutions and form a single phase for any possible composition.[20,21,26,28,29,32] The results of the Rietveld refinement of the XRD patterns of 10 different CANBIC compositions are presented in ESI† (Fig. S3). In Fig. 2b we also provide an empirical linear $L(y)$ relationship allowing to calculate the Bi content in CANBIC perovskites (with x = 0.4) from XRD patterns.

2 Spectral properties of CANBIC perovskites

2.1 Stationary absorption and PL. The absorption band edge of pure CANIC perovskite can be found at *ca.* 3.6 eV with no noticeable absorbance at lower energies (Fig. 3a, curve 1). However, even at a very small amount of Bi introduced into the perovskite, for y = 0.005–0.01, rather dramatic changes can be observed both in absorption and PL spectra. In particular, a new absorption band evolves upon Bi introduction with a distinct maximum at *ca.* 3.4 eV and an edge at *ca.* 3.2 eV (Fig. 3a, curve 2). As the Bi fraction is further increased, this band shifts to lower energies retaining its shape (Fig. 3a, curves 3–10) with the absorption peak and band edge reaching respectively 3.1 eV and 2.8 eV for y = 1.0.

No detectable PL can be found for pure CANIC perovskite under the excitation at 365 nm. When very small amounts of Bi are introduced (y = 0.005–0.01), CANBIC starts to emit PL in a broad band centered at *ca.* 2.2 eV and encompassing the larger portion of the visible spectra range (Fig. 3b). The highest PL intensity was observed for y = 0.01–0.02 decreasing gradually for higher Bi fractions and shifting to lower energies (Fig. 3b, curves 3–10). The development of intense light absorbance and emission upon introduction of minimal amounts of Bi into the CANIC matrix, which otherwise shows a very high energy of the absorption band edge and no PL, are typically interpreted as a result of the Bi species breaking the symmetry of the CANIC lattice and contributing to the formation of CB edge, thus making interband transitions allowed in both directions (light absorption and radiative recombination).[17,18,21,25,26,28,31,32] In terms of this interpretation, Bi^{III} acts as a "key" opening the inherent capacity of the CANIC matrix for light absorption and emission.

The PL excitation (PLE) spectra of CANBICs are very similar to the corresponding absorption spectra, both showing identical positions of band edges depending on y (Fig. 3c). The same energies of band edges derived from absorption and PLE spectra indicate a high structural perfection of the lattice of CANBIC perovskites with no mid-bandgap states originating from defects observed below the edge of the fundamental absorption band. This conclusion is additionally supported by the high quality of the Raman spectra (see discussion below) registered under off-resonance 514.7 nm excitation, showing no PL background despite the very high PL intensity (PLI) of CANBIC samples.

The bandgap E_g of CANBIC perovskites can therefore be evaluated by analyzing both absorption and PLE spectra. Both were found to show linear edges when plotted using the Tauc equation for direct allowed interband electronic transitions, in the case of PLE spectra – as functions of $(PLI \times h\nu)^2$. We followed the dependence of the bandgap on y for three series of CANBIC perovskites with Bi content changing through 3 orders of magnitude (more details are provided below in the discussion of PL QY measurements). The bandgap of CANBIC perovskites was found to decrease monotonously as an almost linear function of the logarithm of the molar Bi^{III} fraction with the $E_g(y)$ dependence overlapping for all three independent sample series (Fig. 3d). Overall, the bandgap of CANBIC perovskites can be precisely tuned between 2.68 eV (y = 1.0) and 3.12 eV (y = 0.005) by changing the Bi^{III} content.

2.2 Discussion of PL origins and factors affecting absolute PL QY. The PL band of CANBIC perovskites is characterized by a relatively large Stokes shift of several hundred meV and by a comparable FWHM of the band (Fig. 3b). Together with a high PL intensity these features indicate that the PL emission of CANBICs originates from a self-trapped excitonic (STE) state. This mechanism is generally typical for lead-free halide perovskites.[9,10,13,17] The STE state is assumed to form due to a strong coupling of the electronic excitation to lattice vibrations resulting in the localization of the exciton on Bi/Ag halide octahedra and a strong distortion of the octahedral geometry. The self-trapped exciton loses a portion of energy needed for

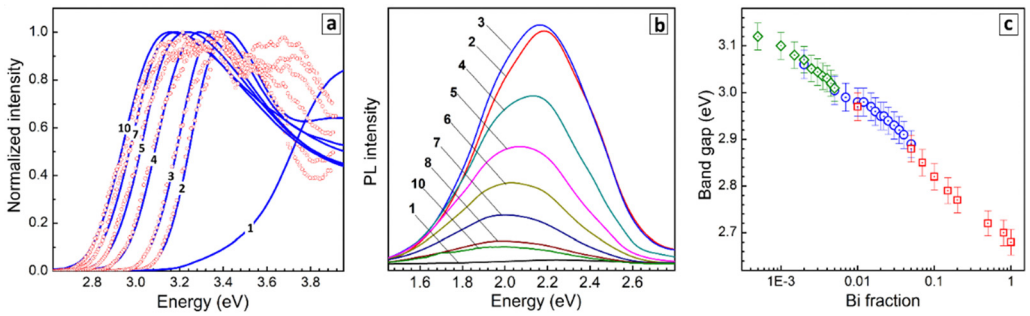

Fig. 3 (a and b) Absorption, PL excitation (a), and PL (b) spectra of CANBIC perovskites with Bi fraction y = 0 (curve 1), 0.01 (2), 0.05 (3), 0.07 (4), 0.10 (5), 0.15 (6), 0.20 (7), 0.50 (8), 0.90 (9), and 1.00 (10). In (a) solid lines are absorption spectra and circles represent corresponding PL excitation spectra. (c) Band gap of CANBIC perovskites as a function of Bi fraction y. A legend for different symbols in (c) is provided in the caption of Fig. 4.

the transition through a potential barrier between free-exciton and STE states as well as lattice reorganization, thus resulting in large Stokes shifts.[9,10,17,18,24,25,28,31,32] The radiative relaxation of the STE state involves multiple phonons due to reversal lattice reorganization and, therefore, the PL is emitted as a series of homogeneously and inhomogeneously broadened phonon replicas of the zero-phonon band which overlap and form a single symmetrical PL band with a FWHM of many hundred meV.[9,10,17,18,24,25,28,32] The STE PL emission can be very efficient, the PL quantum yield (QY) of a particular CANBIC composition reported to be 86% by Sargent's group[18] and as high as 92% recently by us for CANBICs with 2% Bi content.[44]

In the present work, the PL efficiency of CANBIC perovskites was further increased by finely tuning the synthesis conditions. As reported,[44] the post-synthesis ripening of purified CANBIC perovskites at ambient conditions does not change the PL QY for at least six months of shelf storage. However, the duration of the contact of as-precipitated (that is not separated and not purified) CANBIC perovskites with their parental solution which contains excess of Cs^+ and Na^+ was found to have a distinct effect on the PL QY of the final perovskites, produced after the separation from the supernatant and purification.

Fig. 4a shows evolution of the PL QY values measured at room temperature (RT) for different excitation wavelengths as a function of the duration of precipitate ripening in the parental solution before the purification. The PL QY was found to be below 80% for freshly deposited CANBIC-2%, increasing to 92% after 60 min ageing and growing further up to 98% when the ageing was prolonged to 300 min (see insert in Fig. 4a).

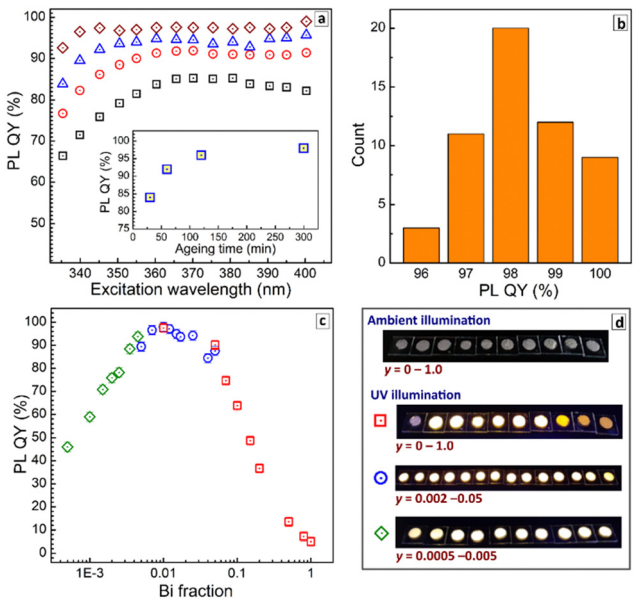

Fig. 4 (a) PL QY of CANBIC-2% perovskite measured at RT and different excitation wavelengths for a sample kept in the parental solution for 30 min (black squares), 60 min (red circles), 120 min (blue triangles), and 300 min (brown diamonds). Inset: PL QY of CANBIC-2% perovskite measured at an excitation wavelength of 365 nm as a function of the ripening duration. (b) A distribution of PL QY values measured for 5 different samples of CANBIC-2% perovskite with excitation wavelengths in the range of 360–380 nm. (c) PL QY of CANBIC perovskites measured at RT as a function of Bi fraction y. (d) Photographs of CANBIC samples with different Bi fractions under ambient and UV illumination.

All probed samples show lower PL QY when excited at 330–340 nm, the emission yield growing to steady values for longer excitation wavelengths. This behavior was attributed to the existence of species absorbing in that spectral range but not contributing to PL emission and resulting, therefore, in lowered PL QYs. A possible candidate for such non-emissive species can be under-crystallized (defective) perovskite on the surface of microcrystals. As the ripening period is increased, the crystallization proceeds and the contribution of these species becomes less pronounced (compare, for example, black squares and brown diamonds in Fig. 4a), while the PL QY grows to a saturation at 98%. The sample aged for 300 min shows a steady PL QY value almost in the entire range of tested excitation wavelengths. No further changes in PL QY were detected for larger ripening times (12 h).

The assumption about incompletely crystallized species affecting the PL QY at excitation in the range of 330–350 nm is additionally supported by a ripening-induced transformation of the absorption spectra (Fig. S4a, ESI†). As the ripening duration is increased from 30 to 300 min the absorbance of the CANBIC sample at 300–340 nm decreases noticeably, while the rest of the spectrum remains mostly unchanged. At the same time, no detectable changes can be observed in the same range in the PLE spectra (not shown). Combining these observations, we can conclude that the ripening results in the extinction of the species contributing to the light absorption but not to the light emission, in accordance with the above arguments.

The reproducibility of the reported synthetic protocol was evaluated by preparing independently four identical batches of CANBIC-2% perovskite and collecting PL QY values for different excitation wavelengths. The samples showed very similar behavior with PL QYs almost converging at the excitation wavelength range of 360–380 nm for all four samples (Fig. S4b, ESI†).

Additionally, samples of ultra-pure $BaSO_4$ powders from three different suppliers (Alfa-Aesar, Sigma-Aldrich, and Thermo-Fisher) were tested as a scattering reference for PL QY measurements. It was found that all PL QY values are very close to each other in the entire excitation wavelength range tested (Fig. S4c, ESI†). An empty cuvette used as a reference expectedly yields much lower PL QY values (Fig. S4c, ESI†) highlighting the importance of a proper scattering reference for the PL QY measurements of highly-luminescent microcrystalline powders.

To evaluate the statistical distribution of PL QYs all values measured for the "champion" CANBIC samples with the highest PL efficiency (x = 0.40, y = 0.01–0.02, at least 300 min of ageing in parental solution) were assembled for several different sample batches. In addition, the PL QY measured at multiple excitation wavelengths (in the range of 350–400 nm) were used for each particular sample as well as data collected using different scattering $BaSO_4$ references. The resulting chart presented in Fig. 4b shows that the champion PL QY at room

temperature is 98 ± 2%. We note that this value is, most probably, the highest one reported so far for microcrystalline CANBIC perovskites with no additional dopants. Similarly high PL QYs of 98–99% were also reported for CANBICs of the same composition (x = 0.4, y = 0.01) but additionally doped with 1% Ni or Ce.[31]

Finally, absolute PL QYs of CANBIC perovskites synthesized with different fractions of Bi^{III} varied from 0 to 1.0 were determined. No noticeable PL was emitted by CANIC sample with y = 0 excited at 365 nm as discussed above while the sample with y = 0.01 showed the highest PL QY of 98%. The PL efficiency gradually decreased almost to zero as the Bi^{III} content is stepwise elevated till y = 1.0 (Fig. 4c, red squares).

To identify more precisely the Bi content at which the maximal PL QY is observed, a second set of samples with y varied from 0.002 to 0.05 was synthesized. This series of CANBICs revealed a high PL QY close to 98% for a rather broad compositional range between 0.8% and 2% Bi^{III} with the PL QY slightly decreasing both for $y < 0.008$ and $y > 0.02$ (Fig. 4c, blue circles).

In view of this behavior, and to collect data on the PL behavior of CANBICs with low Bi content, a third series of samples with y varied from 0.0005 to 0.005 was produced. This series showed a gradual decrease of PL QY with decreasing Bi fraction (Fig. 4c, green diamonds). Photographs of all tested samples made under UV illumination (360–370 nm) are provided in Fig. 4d.

All three dependences of PL QYs overlap and form a unified dependence on the Bi content encompassing a range of more than three decades of y. This dependence shows a plateau at y = 0.008–0.02, where the ultimate PL QY of 98% is observed, and decreases for CANBICs with a lower or a higher Bi content.

Density-functional-theory calculations reported by Manna's group showed that incorporation of $BiCl_6$ octahedra into CANIC introduces localized states below the CB minimum.[25] Due to differences in parity between Bi and In orbitals their mixing is negligible and the photoexcited electron is strongly localized on $BiCl_6$ centers, while the hole is localized on $AgCl_6$ octahedra.[25] Estimations showed that due to the highly localized character of $BiCl_6$ units and typically large lifetime of STE state (>1 μs), the efficiency of the STE emission is expected to be very high even at very low Bi doping level and for a broad range of Bi contents,[25] in accordance with the present observations.

2.3 Probing structure of CANBICs with X-ray photoelectron spectroscopy (XPS). The valence state of the major metal components (Ag, In, Bi) of CANBIC perovskites as well as the position of the VB top were probed by XPS. Inspection of the spectra in the ranges of In3d, Bi4f and Ag3d electron binding energies (Fig. 5a–c for y = 0.02) showed that these cations were present in the expected oxidation states of Ag^+, Bi^{3+}, and In^{3+}. In particular, Ag^+ was identified by its characteristic Ag3d doublet at 367.3/373.3 eV with a characteristic Ag3d doublet splitting of 6.0 eV, Bi^{3+} by the Bi4f doublet at 159.0/164.3 eV with a characteristic splitting of 5.3 eV, and In^{3+} by the In3d doublet at 444.7/452.3 eV with a characteristic splitting of 7.6 eV.[45]

The binding energies of Ag3d and In3d electrons were found to be identical for all CANBIC samples with y varied from 0 to 1.0 (Fig. S5 and Table S2, ESI†). A deconvolution of the Bi4f band into Bi-related components and Cs 4p components (Fig. S5, ESI†) shows bismuth to be present as Bi^{3+} in all CANBIC samples with the same position of the 4f doublet in Bi-rich samples (Table S2, ESI†).

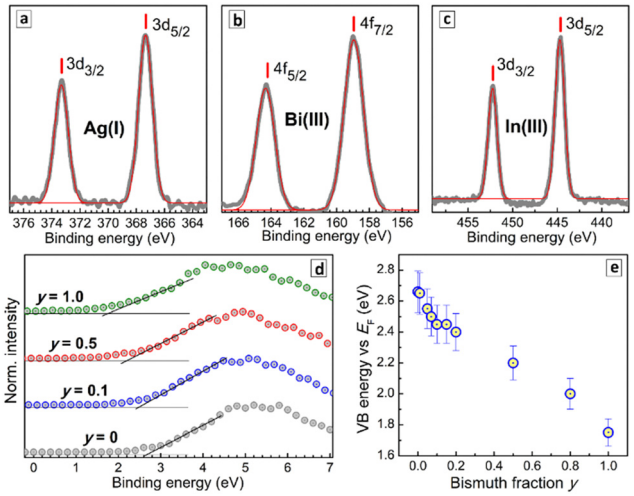

Fig. 5 (a–c) High-resolution X-ray photoelectron spectra of CANBIC perovskite with x = 0.4 and y = 0.5 in the range of Ag3d (a), Bi4f (b), and In3d (c) electron binding energies. Gray lines represent experimental spectra, red lines fits with Gaussian profiles. (d) X-Ray photoelectron spectra of CANBIC perovskites in the VB region. (e) VB energy with respect to the Fermi level E_F as a function of Bi fraction y in CANBIC perovskites.

The VB edge shows a regular shift to lower energies as Bi is introduced into CANIC perovskite and the y fraction increased in CANBICs (Fig. 5d). In particular, the VB edge shifts from 2.66 eV for y = 0 to 1.75 eV for y = 1 with respect to the Fermi level (Table S3, ESI†). The intermediate compositions showed a VB edge energy between these two values (Fig. 5d). The absolute positions of VB and CB edges for all tested CANBIC compositions were calculated by combining the positions of the VB edge recalculated *versus* vacuum level with E_g values derived from absorption/PLE spectra (Table S3, ESI†). Both VB and CB positions were found to shift gradually to lower energies as the content of Bi was increased (Fig. S6, ESI†).

2.4 Probing vibrational properties of CANBIC perovskites by Raman spectroscopy. As noted above, the structural perfection of CANBIC perovskites allows high-quality Raman spectra to be registered under off-resonance 514.7 nm excitation despite the highly efficient PL emission when the excitation energy is in the absorption band.

The Raman spectrum of CANIC perovskite (y = 0) shows three major modes, including an A_{1g} LO phonon band at 300 cm^{-1} and two modes characteristic for vibrations of $InCl_6$ octahedra, namely an E_g(In) at 173 cm^{-1} and a T_{2g}(In) at 144 cm^{-1} (Fig. 6a, curve 1; Fig. S7b, ESI†).[20,21,24,28,32] The Raman spectrum of CANBC perovskite (y = 1.0) has a similar structure, revealing the A_{1g} LO phonon mode at 282 cm^{-1} and two modes characteristic for $BiCl_6$ octahedra, the E_g(Bi) at 219 cm^{-1} and the T_{2g}(Bi) at 114 cm^{-1} (Fig. 6a, curve 10; Fig. S7b, ESI†).[20,21,24,28,32]

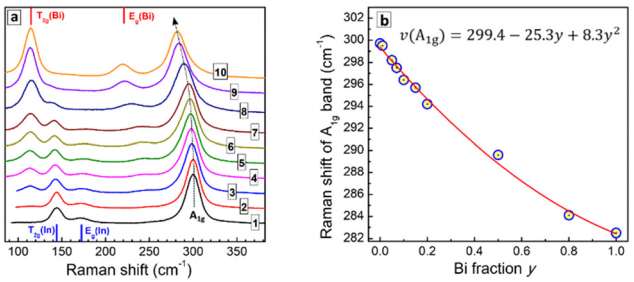

Fig. 6 (a) Raman spectra of CANBIC perovskites with varied Bi fraction y = 0 (1), 0.01 (2), 0.05 (3), 0.07 (4), 0.10 (5), 0.15 (6), 0.20 (7), 0.50 (8), 0.80 (9), and 1.00 (10). (b) Frequency of the A_{1g} mode as a function of Bi fraction y (scatter). Solid red line represents the best fit with a polynominal function "$\nu(A_{1g})$ *versus* y" presented in the figure.

The spectra of Bi-In mixed CANBIC perovskites show in total five modes, including A_{1g}, E_g(In), E_g(Bi), T_{2g}(In), and T_{2g}(Bi). Their positions and relative intensities are proportional to the molar fraction of Bi (Fig. 6a). A clear compositional dependence of the LO mode and Bi, In-related modes, in combination with the high quality of the Raman spectra (high signal-to-noise ratio, no PL background, and high stability of the samples toward laser excitation, *etc.*) make Raman spectroscopy a powerful tool for the identification of the composition of CANBIC perovskites directly from Raman spectra, without the need of additional XRD or EDX analysis. For this purpose different parameters of the Raman spectra can be used, for example, the compositional variation of the LO phonon frequency or energy (Fig. S8a, ESI†), the intensity ratios of E_g(Bi)/E_g(In) and T_{2g}(Bi)/T_{2g}(In) features, or other combinations of composition-dependent parameters (Fig. S8b and c, ESI†).

Fig. 6b shows the dependence of the A_{1g} LO phonon peak frequency on the nominal molar Bi fraction y. The A_{1g} frequency decreases with an increase of the Bi content following a polynomial law. The best fit of the "$\nu(A_{1g}) - y$" dependence is a parabolic expression with a moderate bowing (presented in Fig. 6b), allowing the composition of CANBIC to be identified with good precision in the entire y range.

As the Raman spectra can be measured directly during or after the synthesis, the identification of CANBIC composition using Raman spectroscopy is probably the fastest method among all possible alternatives. Potentially, Raman spectroscopy may be used to probe the formation of double perovskites by the characteristic shape of the spectra. For example, Bi-In perovskites always show a characteristic multi-mode shape of the spectrum with a dominating A_{1g} vibrational band for all CANBICs, even if sodium is completely substituted by silver (Fig. S9, ESI†). However, no spectral patterns characteristic for double perovskites can be found for samples produced without Ag or Cs (Fig. S9a, ESI†), in accordance with corresponding XRD patterns showing the absence of double perovskite phases in such samples.

2.5. Probing photophysical properties of CANBIC perovskites by time-resolved PL spectroscopy. The three series of luminescent CANBIC perovskites encompassing a broad range of y values from 0.0005 to 1.0 were subjected to a time-resolved (TR) PL study at RT. The PL decay curves were registered in the maxima of the corresponding PL bands. For Bi contents higher than 1% the rate of PL decay was found to increase strongly with an increase in the molar fraction of Bi in CANBICs (Fig. 7a). For the range of the smallest Bi contents, at y = 0.0005–0.005, the PL decay rate almost does not depend on the perovskite composition.

The shape of PL decay curves deviates from a single-exponential one with the degree of deviation depending on the Bi content (Fig. 7a). This behavior is typical for lead-free perovskites with STE emission and is assumed to originate from local fluctuations of the lattice structure resulting in a distribution of possible energies of the STE state.[9,10] The transitions between different STE states occur on a fs – ps time scale, *i.e.* much faster than the PL emission events, resulting in the perovskites acting as single-state emitters (like molecules), but with a certain distribution of PL lifetimes, observed as a deviation of the PL decay curves from the single-exponential character.[25,46,47]

In order to collect information simultaneously on the PL lifetime and on the PL decay deviation from the single-exponential decay law, the PL decay curves were fitted using a stretched-exponent model with two fitting parameters – PL lifetime and the heterogeneity parameter h as $I = I_0 \times \exp((-t/\tau)^{1/h})$.[23,47,48] The heterogeneity parameter h is equal to

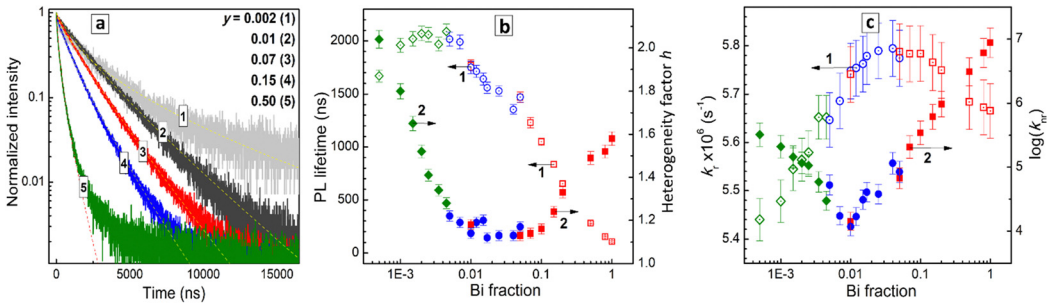

Fig. 7 (a) Kinetic curves of PL decay of CANBIC perovskites with Bi fraction y = 0.002 (curve 1), 0.01 (2), 0.07 (3), 0.15 (4), and 0.50 (5). Dashed lines represent the fitting of the experimental curves with a stretched exponential function. (b) PL lifetime (hollow scatters 1) and heterogeneity factor h (filled scatters 2) derived as functions of y. (c) Rate constants of radiative recombination k_r (hollow scatters 1) and non-radiative recombination k_{nr} (filled scatters 2) as functions of y. Shape of scatters indicates the range of Bi content variation: 0.1 (squares), 0.005–0.05 (circles), and 0.0005–0.005 (diamonds).

1 for the single-exponential PL decay, and larger than 1 for the cases of deviations from the single-exponential decay due to the structural fluctuations.[25,46–48]

Fig. 7b illustrates the dependences of the PL lifetime and heterogeneity factor on the Bi content in a broad composition range covering three orders of magnitude of y variation. The PL lifetime was found to increase from *ca.* 100 ns for pure CANBC perovskite (y = 1.0) up to *ca.* 1600–1700 ns for the most luminescent CANBICs with y = 0.01–0.02 and further to *ca.* 2 μs for compositions with lower Bi content (Fig. 7b, scatter 1). The PL lifetime remains almost constant in the range of y = 0.001–0.008 and decreases for the lowest Bi fraction tested, y = 0.0005, down to *ca.* 1650 ns.

The heterogeneity factor h was found to be at *ca.* 1.6 for CANBC perovskite, decreasing to *ca.* 1.1 for a broad range of compositions encompassing y = 0.01–0.1 (Fig. 7b, scatter 2). At $y < 0.01$ a steady growth of h is observed, reaching above 2.0 for the lowest Bi content of y = 0.0005. These observations indicate that the highest PL efficiencies are observed for the compositional range with the lowest heterogeneity factor, where the PL decay almost obeys the single-exponential law, indicating the highest homogeneity of the perovskite lattice.

The PL lifetime decreases by a factor of almost 20, when the Bi fraction is increased from 1–2% to 100%, evidencing a high probability of the participation of Bi-related structural units of the perovskite lattice in the non-radiative relaxation processes.

By combining the results of TRPL measurements and PL QY values the rate constants for radiative recombination k_r and non-radiative recombination k_{nr} as functions of y (see details in SI) were calculated. The $k_r(y)$ dependence has a dome shape (Fig. 7c, scatter 1) with the rate constant increasing in the range of y = 0.0005–0.08, reaching a broad plateau at y = 0.02–0.08 and decreasing for Bi-richer CANBIC compositions. We note that no drastic changes in the radiative recombination rate were observed for higher Bi contents. The k_r value decreases by only about 25% when y is increased from 0.02 to 1.0. This observation indicates that PL quenching and sharp shortening of the PL lifetime originate from the activation of non-radiative processes in Bi-richer perovskites, rather than from a loss of the emissive capacity.

On the contrary, the rate constant of the non-radiative recombination shows minimal values for the most emissive CANBIC samples and a drastic growth by three orders of magnitude as y is increased from *ca.* 0.01–0.02 to 1.0 (Fig. 7c, scatter 2). By combining the trends of the k_r and k_{nr} changes with the composition, the strong decrease of the PL emission capacity for Bi-richer samples can be assumed to originate from a faster extinction of the STE states in non-radiative processes while the probability of the formation of emissive STE states remains mostly unaffected by the compositional variation.

Conclusions

A new green and single-step approach for the synthesis of microcrystalline $Cs_2Ag_xNa_{1-x}Bi_yIn_{1-y}Cl_6$ (CANBIC) perovskites is introduced. The synthesis is performed under ambient conditions, it does not require *in situ* or post-synthesis thermal treatments, and yields CANBIC powders emitting broadband yellow-white self-trapped excitonic photoluminescence (PL). By using PL as a performance indicator the perovskite composition and the synthesis conditions were tuned to reach the highest possible PL quantum yield (QY) of 98% at room temperature registered for a CANBIC with x = 0.40 and y = 0.01–0.02.

Among other parameters, the duration of ageing of freshly prepared CANBICs in the parental solutions containing an excess of sodium and cesium cations was found to be crucial for reaching near-unity PL QY, most probably due to an increase in the crystallinity and lattice perfection of the CANBIC perovskites. Along with bright PL, CANBICs were found to emit strong visible cathodoluminescence when irradiated with an electron beam.

In the search for the highest possible PL QY the present work focuses on the effect of Bi content (molar Bi fraction y) on the structural, spectral, and photophysical properties of CANBIC perovskites. By applying XRD and Raman spectroscopy the CANBIC perovskites were found to be single-phase products showing an ideal solid solution structure in the entire range of $0 < y < 1$ with In^{3+} isomorphously substituted by Bi^{3+}. Due to high sensitivity of the phonon spectrum to perovskite structure and composition, Raman spectroscopy can be used for an express evaluation of the composition and phase of CANBICs directly during or after the synthesis.

The effect of Bi content on the light absorption and PL properties of CANBIC perovskites was probed on several sets of samples with Bi fraction y varied by three orders of magnitude. The bandgap of CANBICs evaluated both from absorption and PL excitation spectra decreases gradually from 3.12 eV (y = 0.0005) to 2.68 eV (y = 1.0). A similar declining trend was found by XPS also for the valence band (VB) edge with the VB energy decreasing from *ca.* 6.8 eV (*versus* vacuum level) at y = 0 to *ca.* 5.9 eV at y = 1.0.

The room-temperature PL QY showed a dome-shaped dependence on the molar Bi fraction increasing from *ca.* 45% at y = 0.0005 to 97–98% at y = 0.008–0.02 and decreasing at higher Bi contents to a few percent at y = 1.0. For the CANBIC samples with the highest PL efficiency (y = 0.01–0.02) reliable statistics were collected on the absolute PL QY values with several different sample batches, excitation wavelengths, and scattering references, the average value found to be 98 ± 2%.

The room-temperature PL lifetime is close to 2 μs at $y < 0.01$, rapidly decreasing for higher Bi fractions down to *ca.* 100 ns for y = 1.0. The rate constant of the radiative recombination shows only a limited dependence on the Bi content at $y > 0.01$, while the rate constant of non-radiative recombination increases by three orders of magnitude in the same range of $0.01 < y < 1.0$ indicating that $BiCl_6$ octahedra are mostly responsible for the non-radiative recombination of self-trapped excitons.

Author contributions

O. Stroyuk: conceptualization (lead), investigation (equal), writing – original draft preparation (lead); O. Raievska:

investigation (lead), methodology (lead); A. Barabash: investigation (equal), writing – review & editing (equal); C. Kupfer: investigation (equal), A. Osvet: investigation (equal), writing – review & editing (equal); V. Dzhagan: investigation (equal), writing – review & editing (equal); D. R. T. Zahn: resources (equal), writing – review & editing (equal); J. Hauch: conceptualization (equal), project administration (lead), writing – review & editing (equal); C. J. Brabec: conceptualization (equal), funding acquisition (lead), writing – review & editing (equal).

Conflicts of interest

There are no conflicts to declare.

Acknowledgements

O. S., O. R., J. H., and C. B. gratefully acknowledge financial support of The German Federal Ministry for Economic Affairs and Climate Action (project Pero4PV, FKZ: 03EE1092A) and The Bavarian State Government (project ''ELF-PV-Design and development of solution processed functional materials for the next generations of PV technologies'', No. 44-6521a/20/4). CB and AO gratefully acknowledge financial support by the Deutsche Forschungsgemeinschaft under GRK2495/E. VD acknowledges Visiting Scholar program for funding of his research stay at TU Chemnitz. We thank Hamamatsu Photonics GmbH Deutschland (and personally Dr Alexander Kiel) for providing a Quantaurus QY C11347-11 spectrometer for PL QY measurements.

Notes and references

1 A. Dey, J. Ye, A. De, E. Debroye, S. K. Ha, E. Bladt, A. S. Kshirsagar, Z. Wang, J. Yin and Y. Wang, *et al.*, *ACS Nano*, 2021, **15**, 10775.
2 J. Liu, J. Qu, T. Kirchartz and J. Song, *J. Mater. Chem. A*, 2021, **9**, 20919.
3 Z. Xiao, Z. Song and Y. Yan, *Adv. Mater.*, 2019, **31**, 1.
4 M. G. Ju, M. Chen, Y. Zhou, J. Dai, L. Ma, N. P. Padture and X. C. Zeng, *Joule*, 2018, **2**, 1231.
5 J. Shamsi, A. S. Urban, M. Imran, L. De Trizio and L. Manna, *Chem. Rev.*, 2019, **119**, 3296.
6 R. Wang, T. Huang, J. Xue, J. Tong, K. Zhu and Y. Yang, *Nat. Photonics*, 2021, **15**, 411.
7 E. Shi, Y. Gao, B. P. Finkenauer, A. Akriti, A. H. Coffey and L. Dou, *Chem. Soc. Rev.*, 2018, **47**, 6046.
8 N. K. Tailor, S. Kar, P. Mishra, A. These, C. Kupfer, H. Hu, M. Awais, M. Saidaminov, M. I. Dar, C. Brabec and S. Satapathi, *ACS Mater. Lett.*, 2021, **3**, 1025.
9 Z. Xu, X. Jiang, H. Cai, K. Chen, X. Yao and Y. Feng, *J. Phys. Chem. Lett.*, 2021, **12**, 10472.
10 S. Li, J. Luo, J. Liu and J. Tang, *J. Phys. Chem. Lett.*, 2019, **10**, 1999.
11 E.-B. Kim, M. S. Akhtar, H.-S. Shin, S. Ameen and M. K. Nazeeruddin, *J. Photochem. Photobiol., C*, 2021, **48**, 100405.
12 W. Ning and F. Gao, *Adv. Mater.*, 2019, **31**, 1.
13 H. Tang, Y. Xu, X. Hu, Q. Hu, T. Chen, W. Jiang, L. Wang and W. Jiang, *Adv. Sci.*, 2021, **8**, 2004118.
14 Y. Gao, Y. Pan, F. Zhou, G. Niu and C. Yan, *J. Mater. Chem. A*, 2021, **9**, 11931.
15 P. K. Kung, M. H. Li, P. Y. Lin, J. Y. Jhang, M. Pantaler, D. C. Lupascu, G. Grancini and P. Chen, *Sol. RRL*, 2020, **4**, 1.
16 X. Li, X. Gao, X. Zhang, X. Shen, M. Lu, J. Wu, Z. Shi, V. L. Colvin, J. Hu, X. Bai, W. W. Yu and Y. Zhang, *Adv. Sci.*, 2021, **8**, 1.
17 D. Manna, T. K. Das and A. Yella, *Chem. Mater.*, 2019, **31**, 10063.
18 J. Luo, X. Wang, S. Li, J. Liu, Y. Guo, G. Niu, L. Yao, Y. Fu, L. Gao and Q. Dong, *et al.*, *Nature*, 2018, **563**, 541.
19 E. T. McClure, M. R. Ball, W. Windl and P. M. Woodward, *Chem. Mater.*, 2016, **28**, 1348.
20 D. Manna, J. Kangsabanik, T. K. Das, D. Das, A. Alam and A. Yella, *J. Phys. Chem. Lett.*, 2020, **11**, 2113.
21 A. C. Dakshinamurthy and C. Sudakar, *J. Phys. Chem. Lett.*, 2022, **13**, 433.
22 S. E. Creutz, E. N. Crites, M. C. De Siena and D. R. Gamelin, *Nano Lett.*, 2018, **18**, 1118.
23 D. Zhu, J. Zito, V. Pinchetti, Z. Dang, A. Olivati, L. Pasquale, A. Tang, M. L. Zaffalon, F. Meinardi, I. Infante, L. De Trizio, L. Manna and S. Brovelli, *ACS Energy Lett.*, 2020, **5**, 1840.
24 B. Zhou, Z. Liu, S. Fang, H. Zhong, B. Tian, Y. Wang, H. Li, H. Hu and Y. Shi, *ACS Energy Lett.*, 2021, **6**, 3343.
25 F. Locardi, E. Sartori, J. Buha, J. Zito, M. Prato, V. Pinchetti, M. L. Zaffalon, M. Ferretti, S. Brovelli, I. Infante, L. De Trizio and L. Manna, *ACS Energy Lett.*, 2019, **4**, 1976.
26 J. Zhou, X. Rong, P. Zhang, M. S. Molokeev, P. Wei, Q. Liu, X. Zhang and Z. Xia, *Adv. Opt. Mater.*, 2019, **7**, 1801435.
27 Z. Li, F. Sun, H. Song, H. Zhou, Y. Zhou, Z. Yuan, P. Guo, G. Zhou, Q. Zhuang and X. Yu, *Dalton Trans.*, 2021, **50**, 9804.
28 K. Dave, W.-T. Huang, T. Leśniewski, A. Lazarowska, D. Jankowski, S. Mahlik and R.-S. Liu, *Dalton Trans.*, 2022, **51**, 2026.
29 P. Vashishtha, B. E. Griffith, Y. Fang, A. Jaiswal, G. V. Nutan, A. P. Bartók, T. White and J. V. Hanna, *J. Mater. Chem. A*, 2022, **10**, 3562.
30 P. Han, X. Mao, S. Yang, F. Zhang, B. Yang, D. Wei, W. Deng and K. Han, *Angew. Chem., Int. Ed.*, 2019, **58**, 17231.
31 C.-Y. Wang, P. Liang, R.-J. Xie, Y. Yao, P. Liu, Y. Yang, J. Hu, L. Shao, X. W. Sun, F. Kang and G. Wei, *Chem. Mater.*, 2020, **32**, 7814.
32 H. Siddique, Z. Xu, X. Li, S. Saeed, W. Liang, X. Wang, C. Gao, R. Dai, Z. Wang and Z. Zhang, *J. Phys. Chem. Lett.*, 2020, **11**, 9572.
33 S. Li, H. Wang, P. Yang, L. Wang, X. Cheng and K. Yang, *J. Alloys Compd.*, 2021, **854**, 156930.
34 Q. Hu, G. Niu, Z. Zheng, S. Li, Y. Zhang, H. Song, T. Zhai and J. Tang, *Small*, 2019, **15**, 1903496.
35 R. S. Lamba, P. Basera, S. Bhattacharya and S. Sapra, *J. Phys. Chem. Lett.*, 2019, **10**, 5173.
36 Y. Liu, Y. Jing, J. Zhao, Q. Liu and Z. Xia, *Chem. Mater.*, 2019, **31**, 3333.

37 Z. Zhang, Y. Zhang, X. Guo, D. Wang, Y. Lao, B. Qu, L. Xiao and Z. Chen, *ACS Appl. Energy Mater.*, 2022, **5**, 1169.
38 B. Zhang, M. Wang, M. Ghini, A. E. M. Melcherts, J. Zito, L. Goldoni, I. Infante, M. Guizzardi, F. Scotognella, I. Kriegel, L. De Trizio and L. Manna, *ACS Mater. Lett.*, 2020, **2**, 1442.
39 L. Zdražil, S. Kalytchuk, M. Langer, R. Ahmad, J. Pospíšil, O. Zmeškal, M. Altomare, A. Osvet, R. Zbořil, P. Schmuki, C. J. Brabec, M. Otyepka and Š. Kment, *ACS Appl. Energy Mater.*, 2021, **4**, 6445.
40 D. Wu, X. Zhao, Y. Huang, J. Lai, H. Li, J. Yang, C. Tian, P. He, Q. Huang and X. Tang, *Chem. Mater.*, 2021, **33**, 4971.
41 X. Li, S. Xu, F. Liu, J. Qu, H. Shao, Z. Wang, Y. Cui, D. Ban and C. Wang, *ACS Appl. Mater. Interfaces*, 2021, **13**, 31031.
42 D. Huang, H. Xiao, D. Liu, Q. Ouyang, Y. Kong, B. Wang, H. Lian and J. Lin, *J. Mater. Chem. C*, 2021, **9**, 8862.
43 M. Ahmadi, M. Ziatdinov, Y. Zhou, E. A. Lass and S. V. Kalinin, *Joule*, 2021, **5**, 2797.
44 O. Stroyuk, O. Raievska, A. Barabash, M. Batentschuk, A. Osvet, S. Fiedler, U. Resch-Genger, J. Hauch and C. J. Brabec, *J. Mater. Chem. C*, 2022, **10**, 9938–9944.
45 A. V. Naumkin, A. Kraut-Vass, S. W. Gaarenstroom and C. J. Powell, *NIST X-ray Photoelectron Spectroscopy Database*, NIST, 2012.
46 J. E. Thomaz, K. P. Lindquist, H. I. Karunadasa and M. D. Fayer, *J. Am. Chem. Soc.*, 2020, **142**, 16622.
47 R. Chen, *J. Lumin.*, 2003, **102–103**, 510.
48 J. Klafter and M. F. Shlesinger, *Proc. Natl. Acad. Sci. U. S. A.*, 1986, **83**, 848.